Australian Journal of Basic and Applied Sciences, 4(8): 3208-3215, 2010
ISSN 1991-8178

A Three-Dimensional Finite Volume Model for Shallow Water Flow Simulation

Abedini A.A. and Ghiassi R.

Faculty of Civil Engineering, University College of Engineering, University of Tehran,
P.O. Box 11365-4563, Tehran, Iran

Abstract: A three-dimensional cell-centred boundary-fitted finite volume model is developed to solve shallow water equations in open channels. An explicit finite volume method is used to discretize the governing equations in a structured and collocated grid system. A special coupling scheme is applied in some cross-section, based on differences of averaged free surface elevation and flow discharge in 3D model and 1D flow data. The proposed scheme can decrease numerical oscillation and increase the accuracy of the model. The model was applied to simulate 3D flow parameters variation in the developing region of a laboratory flume. Computed 3D velocity profiles were drawn and compared in several cross-sections and layers. Comparing the model results with available experimental data confirmed the efficiency of the scheme.

Key words: 3D model, finite volume, shallow water flow, developing region

INTRODUCTION

Since it is expensive and time consuming to conduct physical model tests and field measurements, many numerical models have been developed and applied to simulate river and open channel flow problems. Most of these models are two-dimensional depth or width averaged models. Depth averaged models provide satisfactory results for many practical purposes. However, they give no information on depth variation of longitudinal velocity and secondary flow; therefore 3D models are necessary to compute all velocity components in three directions. Lane *et al.* (1999) compared predictive ability and accuracy of both 3D and 2D models by using high-quality field data of a gravel-bed river confluence and showed that the 3D model has a higher predictive ability, particularly if the 2D model is not corrected for the effects on flow structure of secondary circulation. The finite difference method has been used extensively to solve the basic governing equations in three-dimensional hydrodynamic models. Because of the rectangular grid, the classic finite difference method (FDM) requires a rather fine mesh size in order to give a satisfactory representation for complicated and curved boundary conditions (Abbott 1979, Chaudhry 1979). All these will lead to a high computational effort. Although the finite element method (FEM) does not always require a regular mesh, it leads to dense matrices and therefore involves lengthy matrix inversion procedures that cause difficulties in recursive calculations of unsteady flow problems (Bauer and Schmidt 1983). The finite volume method (FVM), which has the merits of both FDM and FEM, was apparently introduced first in the field of numerical fluid dynamics, independently by McDonald (1971) and MacCormack and Paullay (1972), for the solution of two-dimensional, time-dependent Euler equations (Hirsch 1988). Recently, Ye *et al.* (1998) developed a three-dimensional hydrodynamic model for free surface turbulent flow using an implicit finite volume method with standard *k-e* turbulence model in a collocated grid.

Chiavassa *et al.* (2003) investigated effects of discretization scheme on a three-dimensional finite volume model of Rhône River plume. Zarrati and Jin (2004) developed a three-dimensional finite volume multi-level model to simulate free surface flows.

In numerical modeling, it is important to obtain an accurate solution with minimum numerical errors. There are several upwind-type and central-type schemes for discretization of convective fluxes which decrease the numerical errors. In this study, instead of using a high-order scheme such as TVD, Osher, Nessyahu-Tadmor, … we have used a simple central scheme with a special coupling scheme that decreases the numerical oscillation without much increasing the numerical efforts (unlike the high-order schemes).

Corresponding Author: Abedini A.A., Faculty of Civil Engineering, University College of Engineering, University of Tehran, P.O. Box 11365-4563, Tehran, Iran
E-mail address: amirabedini@gmail.com

MATERIALS AND METHODS

Main 3D Equations:

Free surface flow can be studied by means of mass and momentum conservation equations (Streeter 1958, Shames 1962, Hirsch 1988). Under the assumption of constant density, hydrostatic pressure distribution and neglecting wind and Coriolis forces, the resulted 3D shallow water equations can be expressed in integral forms as follows (Ghiassi 1995):

$$\oint_s \vec{v}.d\vec{s} = 0 \tag{1}$$

$$\frac{\partial}{\partial t}\int_\Omega u d\Omega + \oint_s u(\vec{v}.d\vec{s}) = -g\oint_s \eta \vec{i}_X d\vec{s} + \frac{1}{\rho}\oint_s \vec{\tau}_X d\vec{s} \tag{2}$$

$$\frac{\partial}{\partial t}\int_\Omega v d\Omega + \oint_s v(\vec{v}.d\vec{s}) = -g\oint_s \eta \vec{i}_Y d\vec{s} + \frac{1}{\rho}\oint_s \vec{\tau}_Y d\vec{s} \tag{3}$$

where, $\vec{v}$ = velocity vector; u and v = velocity components in the horizontal x- and y-directions, respectively; t = time; η = water surface elevation measured from the undisturbed water surface; g = gravitational acceleration; $\vec{\tau}_X$ and $\vec{\tau}_Y$ = components of shear stress tensor in the x- and y-directions, respectively.

Since main idea of the research is to establish a 3D-1D coupling scheme for shallow water flow modeling, a basic algorithm for shear stress evaluation was applied. So, the components of shear stress tensor have been calculated based on Boussinesq approximation, using Prandtl's mixing length model to determine eddy viscosity (Cea *et al*. 2007). The results show that this model which is categorized in zero-equation turbulence models has generally enough accuracy for shallow water flows. However, for investigating a local full 3D flow, more appropriate turbulence models such as two equation k-ε or k-ω or anisotropic turbulence models should be used.

Integrating the continuity equation over the water column together with using kinematic condition at the free surface leads to the following free surface equation (Casulli 1999):

$$\frac{\partial \eta}{\partial t} + \frac{\partial U}{\partial x} + \frac{\partial V}{\partial y} = 0 \tag{4}$$

where, $U = \int_{-h}^{\eta} u dz;\ V = \int_{-h}^{\eta} v dz;\ h =$ water depth from the bed to the undisturbed free surface. This means that H(x, y, t) = h(x, y) + η(x, y, t) is the total depth of water column.

Discretization of Equations:

To solve the governing 3D equations we have used a cell-centred finite volume method on a boundary-fitted structured and collocated grid. At first, computational domain has been divided into a number of hexahedral cells and all geometrical characteristics of cells such as coordinates; surfaces area and volume of cells have been computed. Then, the equations have been discretized for each cell as the following:

$$\sum_{s=1}^{6}\left(u\cdot s_x+v\cdot s_y+w\cdot s_z\right)_s=0 \tag{5}$$

$$\frac{u^{n+1}-u^n}{\Delta t}\Omega+\sum_{s=1}^{6}\left(uu\cdot s_x+uv\cdot s_y+uw\cdot s_z\right)_s= -g\sum_{s=1}^{6}\left(\eta\cdot s_x\right)_s+\frac{1}{\rho}\sum_{s=1}^{6}\left(\tau_{xx}\cdot s_x+\tau_{xy}\cdot s_y+\tau_{xz}\cdot s_z\right)_s \tag{6}$$

$$\frac{v^{n+1}-v^n}{\Delta t}\Omega+\sum_{s=1}^{6}\left(vu\cdot s_x+vv\cdot s_y+vw\cdot s_z\right)_s= -g\sum_{s=1}^{6}\left(\eta\cdot s_y\right)_s+\frac{1}{\rho}\sum_{s=1}^{6}\left(\tau_{yx}\cdot s_x+\tau_{yy}\cdot s_y+\tau_{yz}\cdot s_z\right)_s \tag{7}$$

$$\frac{\eta^{n+1}-\eta^n}{\Delta t}\cdot S_{zt}+\sum_{k=1}^{k\max}\sum_{s=1}^{4}\left(u\cdot s_x+v\cdot s_y\right)_s=0 \tag{8}$$

where, Ω = volume of cell; S_x, S_y and S_z = x-, y- and z- component area of cell faces, respectively and S_{zt} = *z*-component area of top surface of top cell in each water column.

All variables at cell surfaces have been calculated using second-order accuracy central difference scheme as follows:

$$\phi_{i+1/2,j,k}=\frac{l_{i+1}\phi_{i,j,k}+l_i\phi_{i+1,j,k}}{l_i+l_{i+1}} \tag{9}$$

where, φ = *u, v, w, η* and l_i = distance between center of *i* th cell and center of surface *(i+1/2)* in *i* th cell. Same equations are applicable for other surfaces of the cell.

Four different types of boundary conditions have been considered in the model for upstream, downstream, and lateral boundaries of computational domain which included: known velocity, known water surface, open boundary (zero-gradient condition), and closed boundary. At the free-surface, the water flux across the surface was assumed to be zero and the wind stress was ignored. On the bed, the water flux was also assumed zero and a quadratic friction law was used to calculate the bottom shear stress (Henderson 1966).

Solution Procedure:

The overall numerical procedure can be summarized as the following steps:

1. Reading physical domain geometry and generating geometric characteristics of cells.
2. Reading initial flow conditions and the time varying boundary conditions.
3. Reading 1D flow data.
4. Determining wet and dry cells in the computational domain based on water surface elevation *(η^n)*.
5. Solving the free surface equation (8) explicitly to compute η^{n+1}.
6. Coupling 3D model with 1D flow data to reduce oscillation and diminish the increase of computational errors of free surface elevation.
7. Solving the momentum equation in the x-direction (6) explicitly to compute u^{n+1} by using latest values of water surface elevation (η^{n+1}).
8. Solving the momentum equation in the y-direction (7) explicitly to compute v^{n+1} by using latest values of water surface elevation (η^{n+1}).

9. Solving the continuity equation (5) explicitly to compute w^{n+1} by using latest values of horizontal velocities (u^{n+1}, v^{n+1}).
10. Coupling 3D model with 1D data to reduce the increase of computational errors of velocities.
11. Repeating the computation procedure from step 4 to step 10 for next time step.

In a 3D numerical model, a large number of elements are usually defined inside the computational domain and a huge amount of computations are needed for solving governing equations in three directions. Therefore, several kinds of unexpected errors may be increased due to data oscillation, numerical dissipation, and truncation error and so on. These errors which are mostly generated from convective fluxes can cause divergence and instability of the results. Several schemes can be applied for discretization of convective fluxes to decrease the numerical errors such as flux-vector splitting, flux-difference splitting, total variation diminishing (TVD) and fluctuation-splitting schemes (Blazek 2001).

It can be said that any scheme which reduces oscillation and prevent the increase of computational errors, seems to be able to increase stability and accuracy of the results. This idea which can be considered as a coupling scheme has been applied in the present work.

The above-mentioned scheme is based on coupling 3D model with 1D flow data. Two parameters in 3D model, including free surface elevation and total flow discharge have been compared with 1D flow data. In each cross-section, if numerical errors are going to rise, to prevent, 3D results are coupled by 1D flow data. Water surface elevations are treated based on the difference between 1D free surface elevation $(\eta_i)_{1D}$ and 3D average free surface elevation $(\eta_i)_{3D}$ and velocities are treated based on the ratio between 1D flow discharge and 3D flow discharge. Coupling scheme can be applied in each time step or at specific time duration in all cross-sections or some specified sections. All 1D flow data can be obtained from existing numerical models.

The above solution procedure is a combination of second-order central spatial discretization, an explicit multistage temporal discretization and a 3D-1D coupling scheme. Every explicit scheme remains stable only up to a certain value of the time step (Δt). To be stable, an explicit scheme has to fulfill the so-called Courant-Friedrichs-Lewy (CFL) condition. On a 3D structured grid, the CFL condition for a control volume Ω i may be expressed as follows (Blazek 2001):

$$\Delta t_i = C_r \frac{\Omega_i}{(u_i + \sqrt{g h_i})\, s_x + (v_i + \sqrt{g h_i})\, s_y + (w_i + \sqrt{g h_i})\, s_z} \tag{10}$$

where, C_r = CFL number and specified in the range $0 < C_r \leq 1$.

With equation (10), a local time step which is valid for one control volume is obtained. For a global time step for all volumes, a minimum over all volumes is taken.

$$\Delta t = \min(\Delta t_i) \tag{11}$$

In this study, for choosing an appropriate time step that increases the stability, the CFL number is specified about 0.1~0.5.

RESULTS AND DISCUSSION

The numerical model has been verified and validated with flow in developing region test which is commonly used for validation of 3D models. Flow in a developing region is complex, three-dimensional and influenced by secondary circulation and free surface effects. Ranga Raju *et al*. (2000) studied the developing regions in open channels. They measured velocity profiles along the centerline of a 75 cm wide flume at different distances from the inlet. They showed that the dimensionless length (L/h) of the flow-developing region is a function of the flow aspect ratio (h/B) and the channel roughness, where B is the channel width and h is water depth.

Computations were carried out for the same conditions as in the experiment (figure 1), and the simulation results were compared with the available experimental data of Ranga Raju *et al*. (2000). 14 m of the channel length was modeled using a 100×15×19 mesh. A uniform entrance velocity distribution equal to 0.3 m/s was set at the channel inlet.

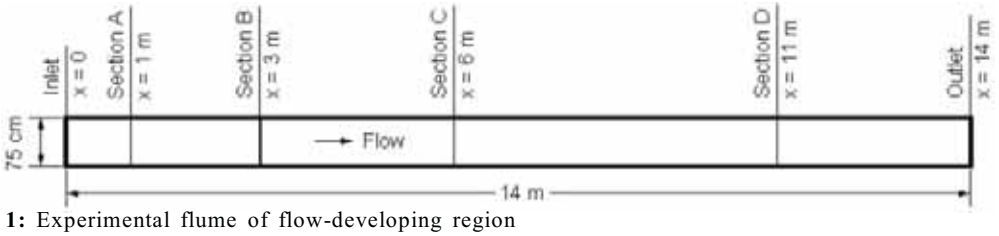

Fig. 1: Experimental flume of flow-developing region

As shown in figure 2, velocity profiles at four different sections in the developing zone were compared with experimental data. There is a good agreement between the model results and experimental data despite using the simple turbulence model.

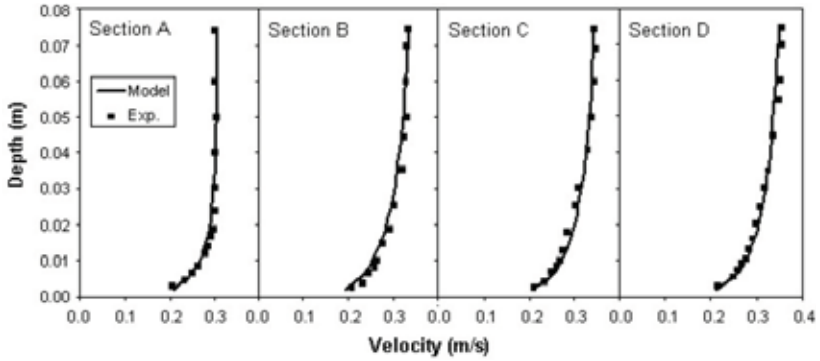

Fig. 2: Comparison of calculated velocity profiles along the developing zone with experimental data

The surface velocity variation along the developing zone was also compared with experimental measurements. Figure 3 shows the good agreement between the model results and experimental data. Comparison between model results with and without the effect of wall friction shows that how boundary layer development at the two side walls creates a flow towards the channel centerline and increase the velocity at the mid section of the channel. Same results were reported by Zarrati and Jin (2004).

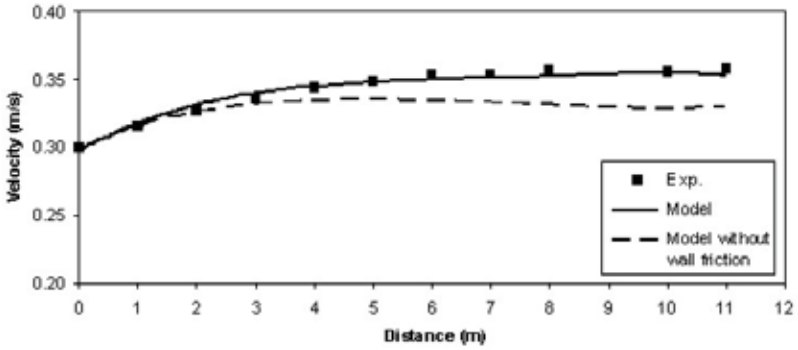

Fig. 3: Comparison of surface velocity along the developing zone with experimental data

Longitudinal velocity vectors at four horizontal layers (z/h=0, 1/3, 2/3 and 1) and five vertical layers (y/B=0, 0.2, 0.5, 0.8 and 1) of flow in developing zone are shown in figures 4 and 5, respectively. Variation of velocities along the length, width and depth of the flow are seen in both figures, despite the fact that constant velocity distribution is specified at the inlet section.

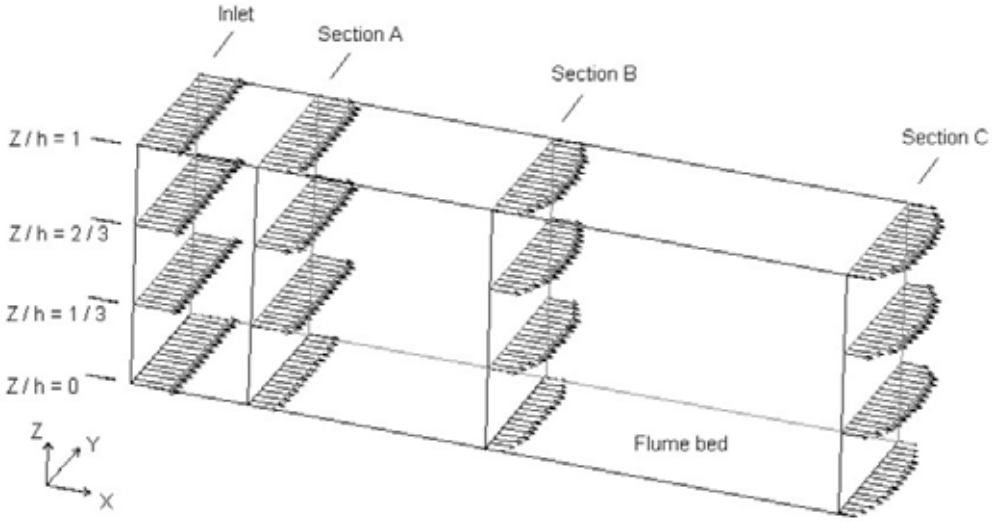

Fig. 4: Longitudinal velocity vectors at four different horizontal layers of flow in the developing zone

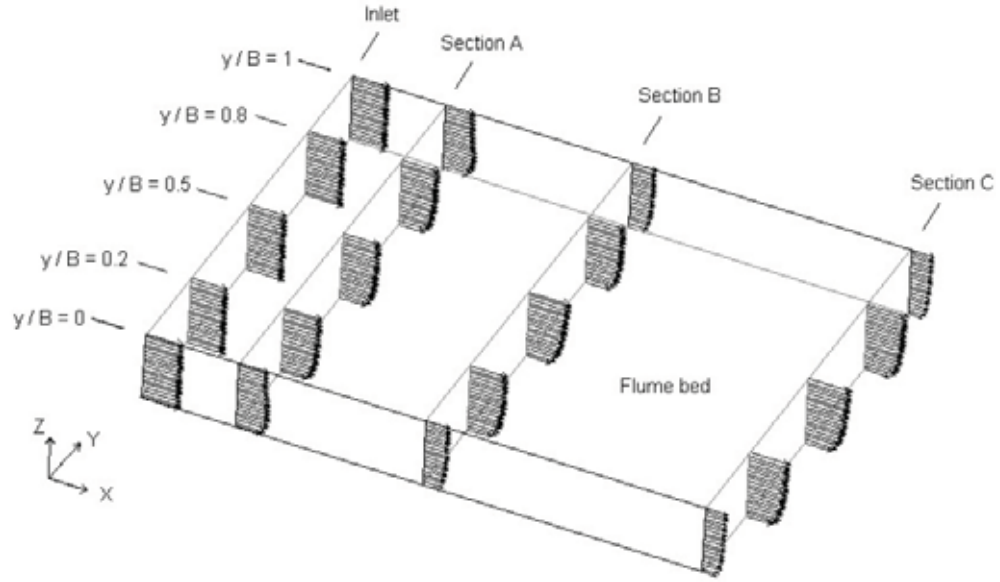

Fig. 5: Longitudinal velocity vectors at five different vertical layers of flow in the developing zone

To investigate the convergence and discretization errors, a grid convergence index (GCI) proposed by Roache (1994) was applied. Hence, flow computations were performed for one additional mesh with 67 ×10×13 cells (designated as coarse mesh). The GCI corresponding to the fine grid solution f_{fine} is defined as follows (Cadafalch *et al.* 2002):

$$GCI_{fine} = F_s \frac{\left|\left(f_1 - f_2\right)/f_1\right|}{r^P - 1} \tag{12}$$

where Fs = 3 is a safety factor; r = grid refinement ratio equal to 1.5 in this test case; p = order of accuracy

that is equal to 2, because of using second-order central spatial discretization and f1 and f2 = an evaluated quantities of the concerned parameters by fine (1) and coarse (2) grids, respectively.

In this example, longitudinal velocities at above mentioned sections are selected as evaluated quantities. The calculations of GCI corresponding to the fine-grid solution have been summarized in Table 1. According to this Table, the maximum numerical uncertainty in the fine-grid solution for longitudinal velocities is equal to 6.21%. As can be seen, for better resolution more mesh refinement is required in the whole water depth.

Table 1: Calculation of Grid Convergence Index at developing region in a rectangular channel

Distance from inlet (m)	GCI_{fine} (%)			Distance from bottom (m)	
	Avearage	Maximum	Minimum	$(z)_{max}$	$(z)_{min}$
1.0	2.62	4.30	1.14	0.015	0.051
3.0	4.21	6.21	1.14	0.063	0.015
6.0	2.13	3.47	1.31	0.004	0.074
11.0	2.27	2.88	1.15	0.074	0.004

To show the advantage of the coupling scheme, a convergence test based on the numerical error history was done for fine grid model in two different courant numbers. As shown in figure 6, for both courant numbers the model without coupling scheme can't converge and especially in courant number equal to 0.2 becomes unstable. While, by applying the coupling scheme the model is stable and converges to the final results.

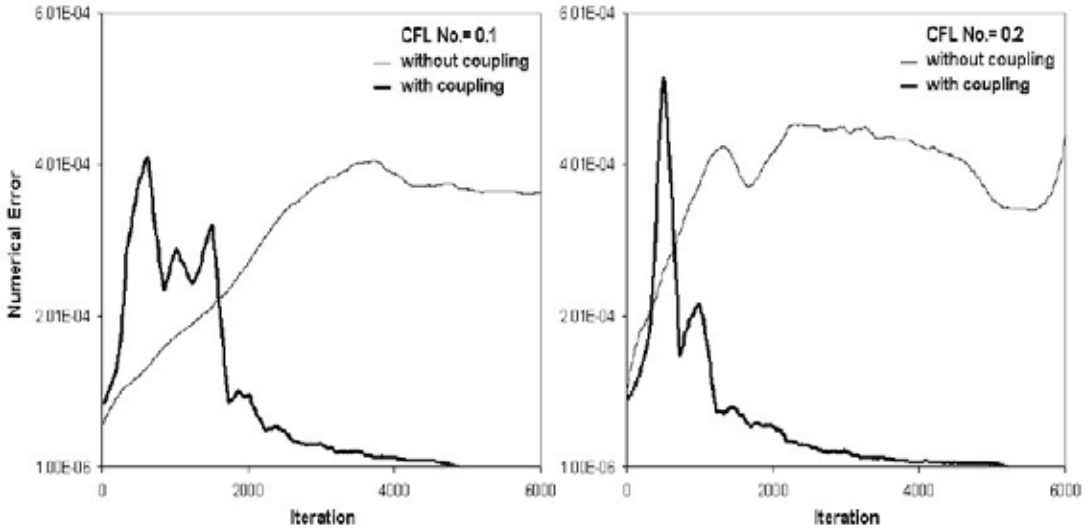

Fig. 6: Numerical error history at flow in the developing zone model

Conclusion:

It was shown that the proposed scheme can increase the efficiency of the model and hence, variation of 3D velocity profiles in a flow developing region of a laboratory flume can be simulated with a good level of accuracy. Based on the achieved results, the coupling scheme can decrease the numerical oscillation and prevent the instability of results.

ACKNOWLEDGMENT

The authors are grateful to Professor A.R. Zarrati of Amirkabir University of Technology for his advice

REFERENCES

Abbott, M.B., 1979. Computational hydraulics: elements of the theory of free-surface flows, Pitman: London.

Bauer, S.W., K.D. Schmidt, 1983. Irregular-grid finite-difference simulation of lake Geneva surge, J. Hydraul. Eng., 109(10): 1285-1296.

Blazek, J., 2001. Computational fluid dynamics: principles and applications, Elsevier Science Ltd, UK.

Cadafalch, J., C.D. Perez-Segarra, R. Consul and A. Oliva, 2002. Verification of finite volume computations on steady state fluid flow and heat transfer. J. of Fluids Eng., 124: 11-21.

Casulli, V., 1999. A semi-implicit finite difference method for non-hydrostatic free-surface flows, Int. J. Numer. Meth. Fluids, 30: 425-440.

Ghiassi, R., 1995. Three dimensional coastal flow modeling using the finite volume method, Phd thesis, University of Bradford, UK.

Henderson, F.M., 1966. Open channel flow, Macmillan Co. Press, New York.

Hirsch, C., 1988. Numerical computation of internal and external flows, Vol. 1, Fundamentals of numerical discretization, John Wiley & sons Ltd.

Lane, S.N., K.F. Bradbrook, K.S. Richards, P.A. Biron, A.G. Roy, 1999. The application of computational fluid dynamics to natural river channels: three-dimensional versus two-dimensional approaches, Geomorphology, 29: 1-20.

MacCormack, R.W., A.J. Paullay, 1972. Computational Efficiency Achieved by Time Splitting of Finite Difference Operators, American Institute of Aeronautics and Astronautics, Paper, 72-154. American Institute of Aeronautics and Astronautics: San Diego, Calif.

McDonald, P.W., 1971. The computation of transonic flow through two-dimensional gas turbine cascades, American Society of Mechanical Engineers, Paper, 71-GT-89. American Society of Mechanical Engineers: New York.

Ranga Raju, K.G., G.L. Asawa, H.K. Mishra, 2000. Flow-establishment length in rectangular channels and ducts. J. Hydraul. Eng., 126(7): 533-539.